



Observation of non-equilibrium fluctuation in the shear-stress-driven hemoglobin aggregates

A. Kabiraj¹, G. Mallik¹, P. P. Dash¹, P. Kumari¹, M. Bandyopadhyay², and S. Rath^{1,a} 

¹ Nanostructure and Soft Matter Physics Laboratory, School of Basic Sciences, Indian Institute of Technology Bhubaneswar, Jatni, Bhubaneswar 752050, India

² Statistical Mechanics Laboratory, School of Basic Sciences, Indian Institute of Technology Bhubaneswar, Jatni, Bhubaneswar 752050, India

Received 12 June 2023 / Accepted 27 November 2023

© The Author(s), under exclusive licence to EDP Sciences, SIF and Springer-Verlag GmbH Germany, part of Springer Nature 2023

Abstract Non-equilibrium fluctuations caused by the rearrangement of hemoglobin molecules into an aggregate state under shear stress have been investigated experimentally. The flow response under the shear stress (σ) corroborates the presence of contrasting aggregate and rejuvenation states governed by entropy production and consumption events. From the time-dependent shear rate fluctuation studies of aggregate states, the probability distribution function (PDF) of the rate of work done is observed to be spread from negative to positive values with a net positive mean. The PDFs follow the steady-state fluctuation theorem, even at a smaller timescale than that desired by the theorem. The behavior of the effective temperature (T_{eff}) that emerges from a non-equilibrium fluctuation and interconnects with the structural restrictions of the aggregate state of our driven system is observed to be within the boundary of the thermodynamic uncertainty. The increase in T_{eff} with the applied σ illustrates a phenomenal nonlinear power flux-dependent aggregating behavior in a classic bio-molecular-driven system.

1 Introduction

The soft colloidal systems (SCSs) have attracted significant attention due to their distinct response from complex fluids in a state of near equilibrium. This is because of the developing phenomena at the level of single organisms [1] as well as over large length and timescales [2, 3]. For example, hemoglobin (Hb) is a globular protein that plays a crucial role in red blood cell function. Through conformational dynamics leading to a change in viscosity, it serves for the maintenance of the nutrition level required for a sustainable life process [4]. Being a protein derivative, the Hb exhibits inter-linkage properties within their tetramer (α - and β -globin) through hydrogen bonding which renders them for the treatment of injuries or disease [5]. Moreover, there is an unconventional aggregated flow observed, even via major arteries, yielding critical health concerns [4, 6]. The Hb SCSs show shears prudent non-linear viscoelastic behaviors in terms of orientation and macro-phase flow [7, 8]. The theoretical studies by L. Mahadevan et al. predict non-equilibrium fluctuation of velocity upon a minimal flow [9]. Again, L. P. Dasi et al. infer shear stress-induced turbulent blood flow linked to energy dissipation against the platelets universality

[10]. Hence, understanding the dynamics of these complex systems (simultaneous presence of multiple interactions in a given system, e.g., the rate of flow of a system against the driven force) is necessary to meet nanobiotechnology's current needs and develop quantifiable measures with predictive capabilities. In common, the fluctuation–dissipation theorem in a system establishes a link between the spontaneous fluctuations at temperature T , and its linear response to an external driving force when it is in an equilibrium state. The aforementioned theory fails to explain the system when it is significantly perturbed to an arbitrary state far from the equilibrium. Inspired by the stimulating results in a sheared hard sphere fluid [11], Gallavotti and Cohen et al. [12, 13] proposed a phenomenal fluctuation theorem to associate with the entropy flux into a system that is sustained in a non-equilibrium (NEQ) steady state by a time-reversible thermostat. Considering the NEQ dynamics in the system [12–14], they propose a functional dependence steady-state fluctuation theorem (SSFT) given by $\lim_{\tau \rightarrow \infty} \frac{P(+S_\tau)}{P(-S_\tau)} = e^{\tau S_\tau}$, where $P(+S_\tau)$ and $P(-S_\tau)$ are the probability of a fluctuation of amplitude S_τ in the rate of entropy production ($+S_\tau$) and rate of entropy consumption ($-S_\tau$) during the finite time interval (τ), respectively. Here, the τ is larger than any microscopic timescale of the system,

^a e-mail: srath@iitbbs.ac.in (corresponding author)

and $S_\tau = \frac{\int_t^{t+\tau} S(t') dt'}{\tau}$, with $S(t')$ being the entropy production rate in the NEQ steady state. When $\tau \rightarrow \infty$, S_τ becomes large referring to $P(+S_\tau) \gg P(-S_\tau)$ states and satisfies classical thermodynamics principle. Moreover, at finite time intervals, the system follows complex fluctuation yielding aggregate states [15], nonlinear fluctuation in velocity of self-propelled polar particles [16], and quantum tunneling current fluctuation [17] for a wide system ranging from macro- to nanoscale regime. According to the fluctuation theorem, a driven system in a large fluctuation state may have a negative rate of work done. It implies that the driven-dissipative system could temporarily feed energy back into the power supply (source). Nevertheless, the second law of thermodynamics and Jarzynski equality [18] are frequently applied in a variety of NEQ processes to understand the fluctuation. The pioneering experimental work by A. K. Sood et al. [19] demonstrated the above NEQ process using a large volume sheared micellar gel in the presence of global flux. Moreover, thanks to the recent development in stochastic thermodynamics which relates the fluctuation of lower bound observables by thermodynamic uncertainty relation (TUR) [20–22], and validation of the TUR needs strong experimental evidences in a variety of system [23].

In this report, we have explored the dynamics of the Hb system under low shear. Our investigations in the sheared Hb SCSs under ambient conditions (temperature ~ 300 K) resulted in—(i) nonlinear flow bounded to an aggregate state; (ii) the flow dynamics are discussed using non-equilibrium fluctuation theorem characterized through the rate of entropy production and consumption; and (iii) the validity of TUR is looked at to unfold boundary of the driven soft colloidal system.

2 Experimental

2.1 Materials

The lyophilized bovine hemoglobin powder, ethylenediaminetetraacetic acid (EDTA) and phosphate-buffered saline (pH 7.2) used for the sample preparation, were purchased from HiMedia, India, and Sigma-Aldrich, respectively.

2.2 Preparation and stability of hemoglobin (Hb) dispersion

The Hb SCSs were prepared using lyophilized bovine hemoglobin powder and phosphate buffer solution (PBS) at pH 7.2 in the presence of anticoagulant EDTA. For a typical sample preparation, 1 mg of Hb was dispersed in 1 ml of the PBS containing 13 μg of EDTA using a vertex shaker operating at 200 RPM for a duration of 30 min. Throughout the procedure, a temperature of 300 K was maintained. The stability of the

solution was verified from the optical absorption analysis using a UV–VIS Shimadzu (UV-1800) spectrophotometer. All rheological experiments were done at 300 K within the stability period specified in supporting information (SI).

2.3 Rheological method

The flow dynamics of the samples have been studied using a stress-controlled rheometer MCR 301 (Anton Paar, Austria) with a parallel-plate (PP) geometry ($\Phi \sim 50$ mm and gap ~ 110 μm) having an angular resolution, 0.01 μrad at temperature, 300 K. A Peltier hood is affixed to the rheometer instrument in order to regulate the operational temperature and mitigate sample evaporation during the measuring process. For rheological studies, a sample of volume 3.8×10^{-7} m^3 was used and necessary measures have been taken to rule out the bubble-mediated artifact and slippage. The steady-shear flow behaviors and the shear start-up experiments were analyzed in the shear rate range from 0.005 to 100 s^{-1} over a time period of 700 s. The frequency sweep study at a stress amplitude of 0.003 Pa under oscillatory shear has been carried out to justify the viscoelastic nature of the sample. The shear rate versus time fluctuations data at a constant stress have been acquired for a correlation time of 40 ms. It is worth noting that the shear rate in PP geometry exhibits radial variation from the center of the plate when a noticeable gap exists between them. However, this issue can be minimized by selecting a very small gap. Furthermore, the ongoing studies are based on the statistical mean of shear rate fluctuation rather than its absolute magnitude. Hence, the above PP arrangement is deemed appropriate for the conducted measurements. Similar experimental geometry has been used by different researchers [19] for the NEQ fluctuation studies.

3 Results and discussion

3.1 Complex flow behavior

The flow curves of the sample have been investigated at controlled shear rate (CSR) mode, and the results are shown in Fig. 1. From the viscosity versus shear rate plot (indicated by the left black arrow) shown in Fig. 1a, it exhibits a shear thinning behavior [24, 25]. Further, the shear stress versus shear rate plot (indicated by the right gray arrow) as shown in Fig. 1a follows distinct (i) linear, (ii) onset of shear thinning, and (iii) plateau regimes. The characteristics of linear and plateau regimes were analyzed with two start-up experiments [26, 27] for $\dot{\gamma} = 0.08$ s^{-1} and $\dot{\gamma} = 8$ s^{-1} , which are shown in Fig. 1b, c, respectively. Interestingly, the stress of the sample in the linear regime reaches a constant value of 0.035 Pa after a transient state [27, 28] over a time period of 600 s. This demonstrates a steady-state-bound incremental behavior of stress. But, the average

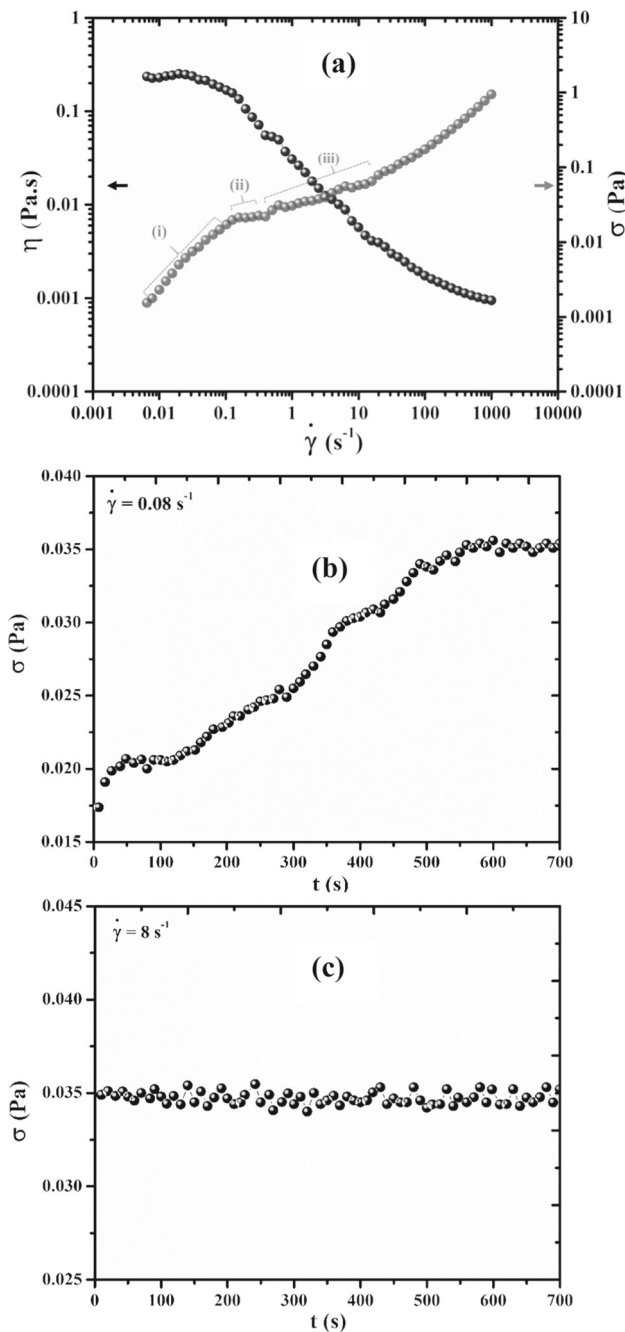


Fig. 1 a Viscosity, η , versus shear rate, $\dot{\gamma}$, and stress, σ , versus shear rate, $\dot{\gamma}$, plots of the sample indicated by dark and gray solid spheres, respectively. The stress curve marked by (i), (ii), and (iii) represents the linear, onset of shear thinning, and plateau regime, respectively. Stress, σ , versus time, t , plot at a constant b shear rate 0.08 s^{-1} and c shear rate 8 s^{-1} , respectively

stress in the plateau regime is observed to be constant over the whole time period analogous to the granular system. Therefore, the transient behavior in the linear region behaves like a yield stress fluid at the macroscopic scale. This confirms the presence of a steady state [29–31] consisting of coexistence of fluid-like and solid-like states that are prone to intriguing structural

rearrangement. Again, to understand the response of the samples (e.g., velocity gradient between two adjacent layers with time) to variable shear stress, the stress sweep measurements have been carried out with a waiting time period of the 20 s. Figure 2a shows the average shear rate, $\langle \dot{\gamma} \rangle$ versus shear stress, σ plot at room temperature, 300 K. Here, we noticed two distinct regimes of velocity gradient, the stress sweeps (i) up to 0.004 Pa, showing a subtle change in $\langle \dot{\gamma} \rangle$ and (ii) beyond 0.004 Pa, a swift rise in $\langle \dot{\gamma} \rangle$, resulting a conventional flow behaviors indicated by regime-I and regime-II, respectively. A well-defined boundary (marked by a blue dotted line) in the metric of stress refers to the aggregate state [19, 32], and the rejuvenation state [32, 33], respectively (for microscopic images see supporting information (SI)). The viscoelastic nature of the sample in regime-I was studied through frequency sweep, and the plots are shown in Fig. 2b. The storage modulus (G') and loss modulus (G'') are marked by the filled blue and black open diamond, respectively. The trace of the modulus under oscillatory shear reveals the dominance of the solid-like phase ($G' > G''$) as demanded of an aggregate state. To investigate the degree of frequency dependent viscoelastic moduli, G' and G'' are fitted with a power law given by, $G' \sim \omega^n$ and $G'' \sim \omega^m$. From the fitting, the n and m values are found to be 1.75 and 0.55, respectively. In contrary to the G'' , the higher-order power-law behavior of G' predicts interconnected aggregate state. The loss tangent ($\tan \delta \sim G''/G'$) approaching 0.07 indicates the weak linkage of the aggregates [34]. Notably, the sheared fluid with $\tan \delta < 0.1$ refers the gel state [35]. The crossover frequency at 0.78 rad/s predicts the mean free relaxation time ($t_r = \frac{2\pi}{\omega}$) as 8.05 s.

3.2 Fluctuations analysis of aggregate state

The statistical properties of the sample have been analyzed in the framework of relaxation phenomena. The instrumental time resolution for the fluctuations studies is 40 ms. Figure 2c, d shows the shear rate fluctuations versus time plots of the sample in an ‘aggregate state’ (i.e., sample brought to the regime-I by a requisite shear stress) for a typical time frame 1–400 s and 650–900 s, respectively. The white solid line and red dotted line represent the zero-shear rate reference line and mean value of the shear rate fluctuations. The time-dependent shear rates studies, shown in Fig. 2c, d, exhibit an initial aging (shear rate decreases with time) up to 50 s followed by a near steady-state fluctuations in the time frame 1–400 s and a typical steady state in the time frame 650–900 s, respectively, at a constant $\sigma = 0.0035 \text{ Pa}$. The observation of initial aging may be due to the process of sample transferring and loading into the rheometer leading to unavoidable mechanical shearing. In order to get a reproducible initial condition, we follow a given preshear protocol: (1) A small constant shear rate of 0.01 s^{-1} for 300 s has been applied after loading the sample into the rheometer and (2) to achieve the rejuvenation state, a stress 5 Pa more than

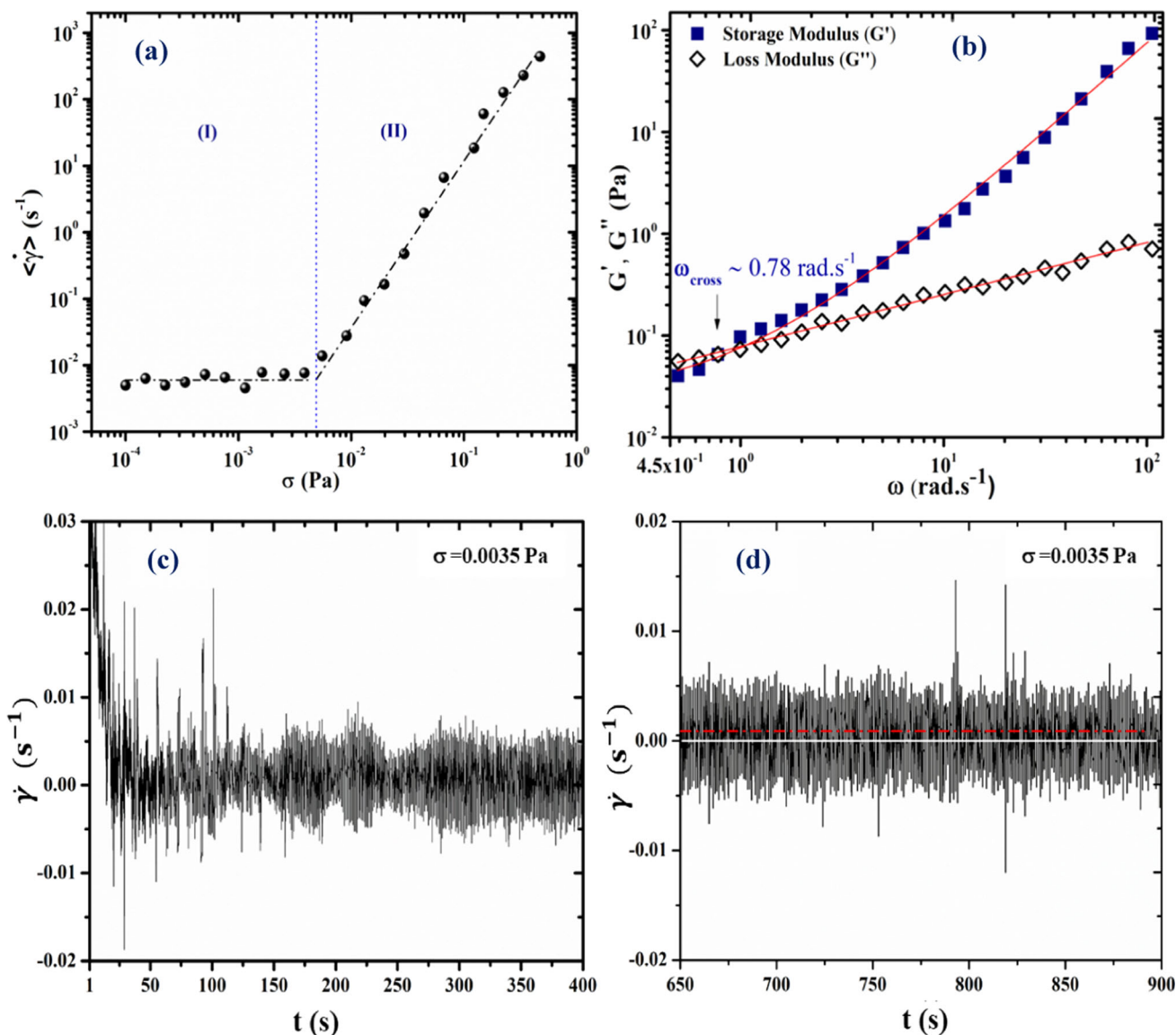


Fig. 2 a Average shear rate ($\dot{\gamma}$) versus shear stress (σ) plot of the sample. The blue dotted line indicates the boundary of aggregate (regime-I) and rejuvenation (regime-II) phase. b Storage modulus, G' and loss modulus, G'' versus angular frequency, ω , at a stress amplitude 0.003 Pa, in regime-I.

$G' \sim \omega^n$ and $G'' \sim \omega^m$ fit are shown in continuous red line. c, d are the shear rate fluctuation versus time plot for $\sigma = 0.0035$ Pa in a typical time window 1–400 s and 650–900 s, respectively. The white line and dotted red line represent the zero reference and mean of fluctuation respectively

the yield stress for 300 s has been imposed. After completion of these processes, shear rate fluctuation data have been gathered for the applied stress corresponding to sample’s aggregate state. Notably, for a specified shear stress condition, the shear rate fluctuations have started to monitor after a waiting period of 100 s. The dynamic of the fluctuations in the aggregate state has been examined under the global power flux [17, 19] at a time “ t ” maintained from the rheometer drive to the system given by $p(t) = \sigma(t)V_s\dot{\gamma}$. Here, V_s , σ , and $\dot{\gamma}$ are the volume of the sample, shear stress, and shear rate, respectively. Again, in the presence of applied global flux, the generalized entropy production of the system

can be written as $s(t) = \frac{p(t)}{k_B T_{eff}}$. The shear rate fluctuations versus time, “ t ” plot in the regime-I for two different stress values, 0.002 Pa and 0.0025 Pa, are shown in Fig. 3a, b, respectively. Interestingly, it demonstrates a steady-state fluctuation of shear rates around zero (marked by white solid lines) with a mean positive values, $2.352 \times 10^{-3} \text{ s}^{-1}$ and $5.377 \times 10^{-3} \text{ s}^{-1}$ (indicated by red dotted lines), respectively. In order to comprehend the probability distributions functions (PDFs) of the system, let us define a normalized variable equivalent to the rate of work done, $W(t) = \frac{s(t)}{\langle s(t) \rangle} = \frac{\dot{\gamma}}{\langle \dot{\gamma} \rangle}$ and $W_\tau = \frac{1}{\tau} \int_t^{t+\tau} W(t') dt'$. In terms of entropy, the same equation

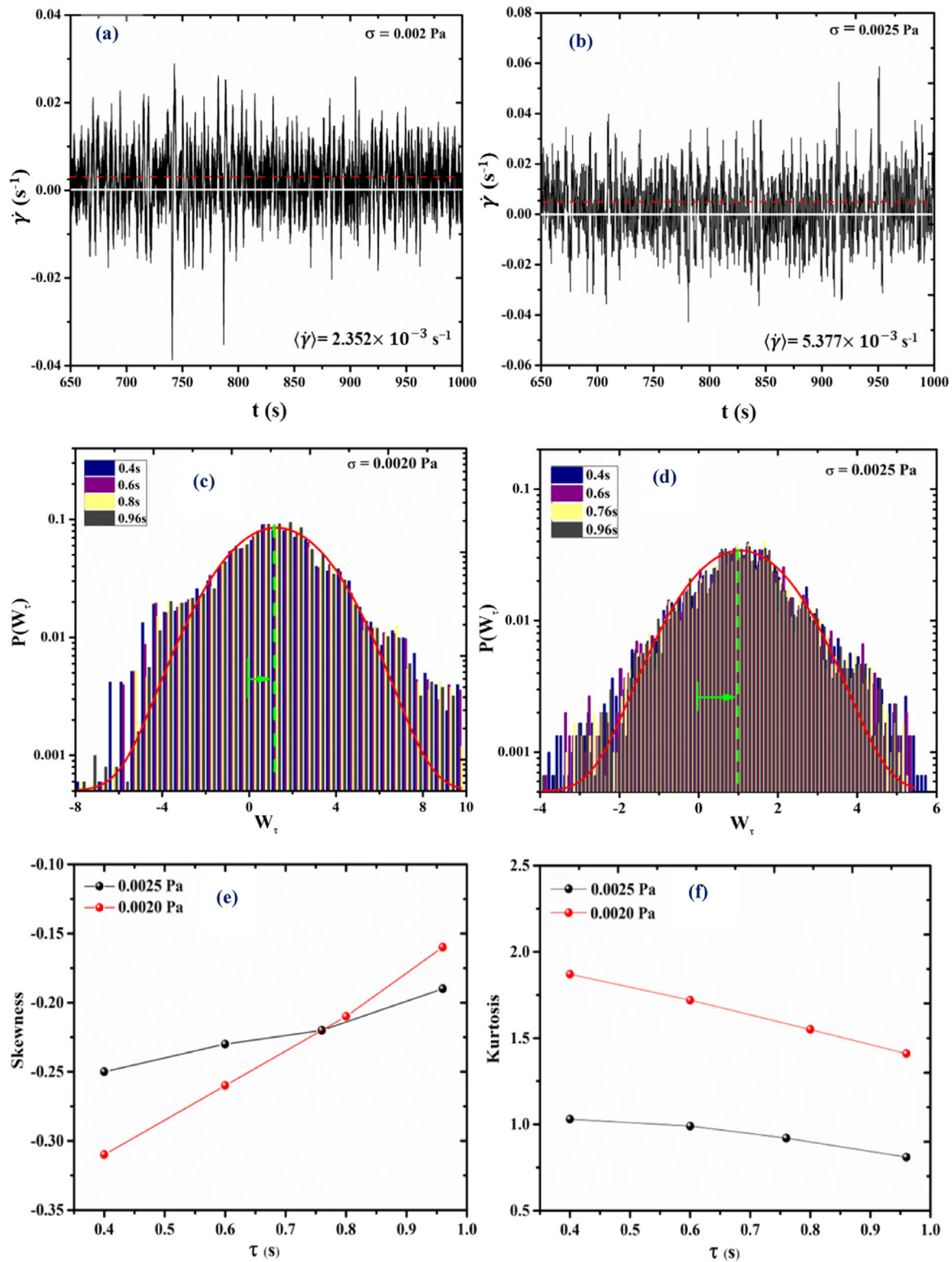


Fig. 3 Shear rate fluctuation versus time, t , plot for **a** stress, $\sigma = 0.0020$ Pa, and **b** stress, $\sigma = 0.0025$, in a typical time window 650–1000 s, respectively. The white line and dotted red line represent the zero reference and mean of shear rate fluctuations, respectively. **c**, **d** are the probability distribution, $P(W_\tau)$ versus W_τ plot for the fluctuation (**a**, **b**) over the time bin, $\tau = 0.4, 0.6, 0.8, 0.96$ s. The continuous

red line is a Gaussian fitted curve. The dotted green vertical line indicates the shift in Gaussian peak position from zero (measure of shift is represented by green horizontal arrow). **e** Skewness versus. τ Plot and **f** kurtosis versus. τ Plot of the distributions for two different shear stresses 0.0020 Pa and 0.0025 Pa, respectively

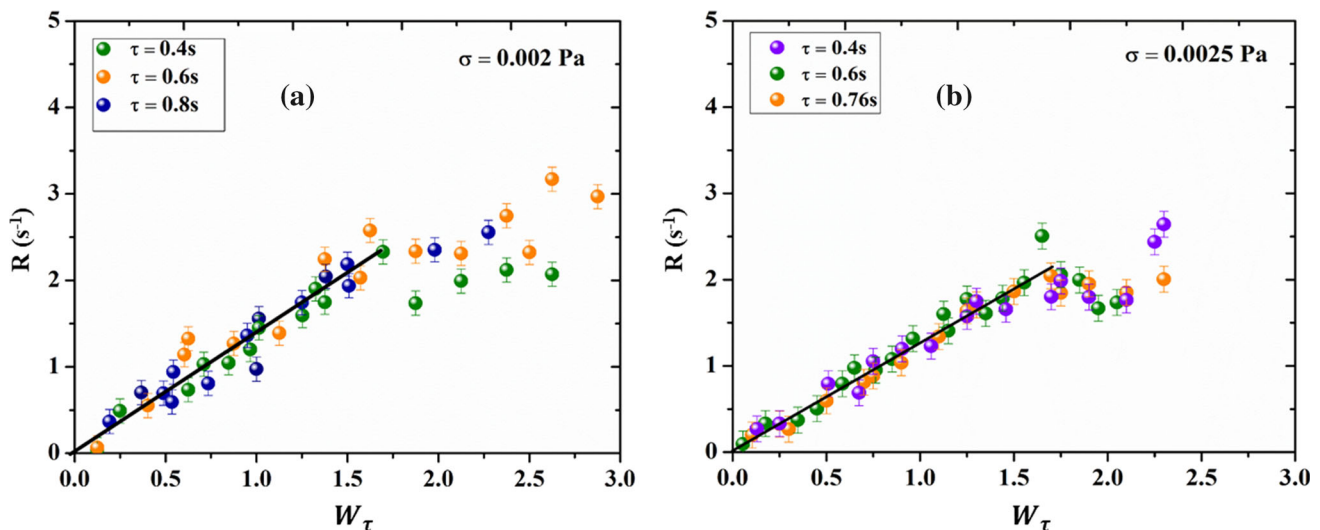


Fig. 4 Master curves, R versus W_τ for the **a** shear stress 0.0020 Pa and **b** shear stress 0.0025 Pa, respectively. The linear regression passing through origin (continuous black line) satisfies the SSFT

can be rewritten as $W_\tau = \frac{s_\tau}{\langle s(t) \rangle} = \frac{1}{\tau \langle s(t) \rangle} \int_t^{t+\tau} s(t') dt'$, and $\langle s(t) \rangle = \frac{\sigma(t) V_s \langle \dot{\gamma} \rangle}{k_\beta T_{\text{eff}}}$. Figure 3c, d shows the PDFs versus W_τ plots corresponding to the stress values 0.0020 Pa and 0.0025 Pa, respectively. The experimental data have been analyzed using the $W(t)$ series for different binning times, τ which is extracted from the $s(t)$ series. To ensure the statistical accuracy and the independent sampling, the overlapping bins and the bin's center shift (center of each bin is shifted from the previous one by a time difference 0.2 s which is larger in comparison with the correlation time ~ 0.04 s) methods are used, respectively. The similar statistical methodology has been used for fluctuations studies of various micro- to macro-system [15, 36, 37]. The probability distribution of W_τ , i.e., $P(W_\tau)$, ranges $-W_\tau$ to $+W_\tau$ indicating entropy consumption and production events, respectively. It is noteworthy that (i) the entropy consumption (negative rate of work done) events are the characteristic signatures of the non-equilibrium process in contrast to the thermodynamically favorable entropy production events and (ii) finiteness of the net entropy production events permit the statistical relaxation process without violating the second law of thermodynamics. The PDFs are fitted with a Gaussian function, $P(W_\tau) = \frac{1}{\sqrt{2\pi}} e^{-\frac{(W_\tau - \langle W_\tau \rangle)^2}{2\Gamma^2}}$, where $\langle W_\tau \rangle$ and Γ are the mean and the standard deviation of W_τ time series, indicated by continuous red lines, respectively. Again, the measure of non-Gaussianity with time binning has been estimated from the rate of work done for two different shear stress 0.002 Pa and 0.0025 Pa through the skewness, $S = \frac{\langle (\partial W_\tau)^3 \rangle}{\alpha^3}$, and kurtosis, $K = \left[\frac{\langle (\partial W_\tau)^4 \rangle}{\alpha^4} - 3 \right]$, where $(\partial W_\tau) = [W_\tau - \langle W_\tau \rangle]$ and $\alpha^2 = \langle \partial W_\tau^2 \rangle$ [16], and the plots are shown in Fig. 3e, f. Here, the skewness gradually increases from -0.3 to -0.1 with increment in τ indicating the negative nature

of distribution (peak) spread out from Gaussian (i.e., degree of asymmetry in the distribution) along x-axis. The negative value of skewness indicates asymmetric tailing of distribution toward negative x-axis that shifts the center toward right. Similarly, the decrease in kurtosis from 2 to 0.5 with τ reveals the appearance of light tail and steep (decrease in flatness) peak of the distribution, compared to the normal one. The observed nonzero skewness and kurtosis ($S \neq 0 \neq K$) refer to a non-Gaussian characteristic contrary to the Gaussian distribution ($S = 0 = K$). From the above analysis, it is confirmed that the system approaches the thermodynamical relaxation process for very large τ as predicted by the SSFT. According to Sood et al. [19], the cylindrical micellar gel follows an increase in non-Gaussianity with stress, which may be due to deformation in the structure. Moreover, our Hb sample is more like globular inter-linked aggregate state. The decrease in non-Gaussianity with shear stress may be of structural origin. Further, under two different aforementioned conditions, the central line of the PDFs has been shifted forward to 1.207 and 1.057, respectively, in contrast to the Gaussian distribution. Again, the peak shift decreases with increasing global flux (increase in shear stress), leaving a finite probability in the negative W_τ regime. This illustrates phenomenal (i) the entropy consumption (a decrease in entropy during the interaction of the system with the surrounding contradicting the second law of thermodynamics) and (ii) the finite probability in positive W_τ represents the entropy production (an increase in entropy during the interaction of the system agreeing the second law of thermodynamics) events. These events typically occur when the driven system is far from its equilibrium condition within a microscopic timeframe shorter than the relaxation time. The intricacy of the interaction mechanism can further be unfolded in a large τ limit through a normalized variable, $R = \frac{1}{\tau} \ln \left[\frac{P(+S_\tau)}{P(-S_\tau)} \right] = \frac{1}{\tau} \ln \left[\frac{P(+W_\tau)}{P(-W_\tau)} \right] = s_\tau = W_\tau \langle s(t) \rangle$ as

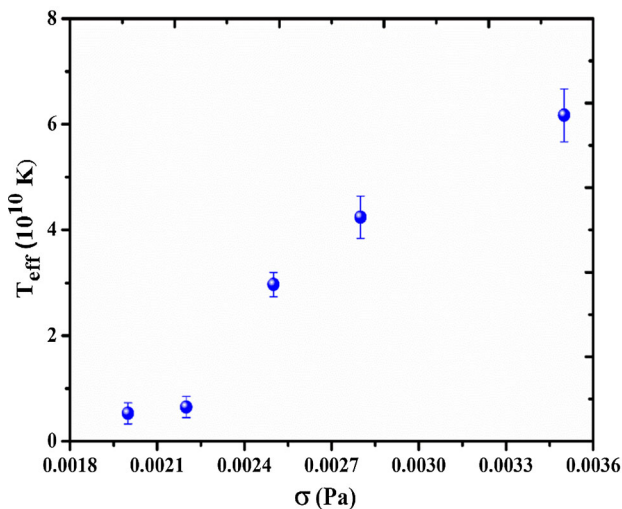


Fig. 5 Effective temperature, T_{eff} , versus applied stress, σ , in the aggregate states of the sample

Fig. 4a, b shows “ R ” versus W_τ plots of the two different power fluxes that scale down to a single master curve over a large range of time binning (400 ms to 1000 ms). The normalized distribution is fitted with a straight line shown by a continuous black line. The linear regression line is passing through origin, agreeing with the time-independent SSFT up to the $W_\tau \leq 1.75$, as stated by the Gallavotti and Cohen theory. Similar characteristics have been observed in different systems as reported by N Kumar et al. [16] and S. Majundar et al. [29]. From the linear fit, the average entropy generation has been estimated to be $\langle s(t) \rangle = (1.7535 \pm 0.096) \text{ s}^{-1}$ and $(1.2517 \pm 0.089) \text{ s}^{-1}$, respectively. For $W_\tau > 1.75$, the behavior of the system is deviated from SSFT resulting a time-evolved non-equilibrium state. Further, when the system is far from equilibrium (aggregate, chaotic, etc.), the overwhelming instantaneous change in the average entropy within the relaxation time period is proportional to T_{eff} [19, 38, 39]. This reflects the energy scale of the system defined in the spirit of shear-stress-driven fluctuations of the Hb–dispersion system analogs to “Jammed states” reported in various articles [15, 19]. From the above fitting, T_{eff} has been estimated as $(9.441 \pm 0.236) \times 10^{10} \text{ K}$ and $(29.713 \pm 0.422) \times 10^{10} \text{ K}$ for two different shear stress conditions ($\sigma = 0.0020 \text{ Pa}$ and $\sigma = 0.0025 \text{ Pa}$), respectively. Figure 5 shows the T_{eff} versus applied stress (σ) plot in the regime-I. The T_{eff} shows ascending behavior with applied stress. It may be due to the system-dependent increase in stress rate fluctuations attributing to athermal steady-state fluctuations. Many NEQ systems have a similar T_{eff} which can be interpreted in an energy scale as a large amount of participating constituents exhibit velocity gradient fluctuations in comparison with the Brownian system [29]. The high values T_{eff} consorted with the energy scale of the fluctuations set by applied stress. The T_{eff} observed from our system is in concurrence with the studied macroscopic to nanoscopic NEQ systems [15, 17, 19, 40].

Table 1 TUR calculation chart for different shear stresses that fall in the regime-I at different binning times

Stress values (σ)	Time bin values (τ)	TUR, $\frac{\text{Var}(W_\tau)}{\langle W_\tau \rangle^2}$	$\frac{\text{Var}(W_\tau)}{\langle W_\tau \rangle^2} \geq \frac{2k_B}{\langle S \rangle}$
0.0020 Pa	0.4 s	1.091	$\geq 0.506 k_B$
	0.6 s	0.942	
	0.76 s	0.765	
	0.96 s	0.608	
0.0025 Pa	0.4 s	2.438	$\geq 1.5978 k_B$
	0.6 s	2.063	
	0.76 s	1.997	
	0.96 s	1.906	
0.0028 Pa	0.4 s	10.868	$\geq 2.759 k_B$
	0.6 s	10.570	
	0.76 s	10.313	
	0.96 s	9.962	

3.3 Validation of the TUR

The thermodynamic uncertainty relation (TUR) specifies the trade-offs between fluctuations and thermodynamic cost for the universal limit. For example, the TURs impose strict restrictions on the fluctuations of thermodynamic currents. It predicts the dissipation constraints through current fluctuations (e.g., heat, work, particles, etc.) of a steady state by driving out far from equilibrium [20, 22]. The W_τ is analogous to the rate of work done exchanged during an out-of-equilibrium process over some generic time interval. According to the TUR, the bound signal-to-noise ratio (SNR) of W_τ is given by $\frac{\text{Var}(W_\tau)}{\langle W_\tau \rangle^2} \geq \frac{2k_B}{\sigma_s}$, where $\text{Var}(W_\tau) = [\langle W_\tau^2 \rangle - \langle W_\tau \rangle^2]$ refers to the variance, $\langle W_\tau \rangle$ is the average work, and σ_s is the average entropy production $= \langle S \rangle$, with Boltzmann’s constant $k_B = 1$ [20–23]. The TUR inequality under different global fluxes is listed in Table 1. From our sample, it has been found that the dynamical phase is in agreement with the TUR and the universal bound. This gives the quantitative nature of NEQ fluctuations in a bio-molecular complex system.

4 Conclusions

In conclusion, the flow dynamics of the shear-stress-driven Hb system reconciled to the presence of two distinct aggregate and rejuvenation phases. The shear rate (velocity gradient) fluctuation in the aggregate phase exhibits phenomenal system-to-surrounding interaction due to the exchange in elastic energy powered by the global power flux. The non-Gaussian nature and positive peak shift (away from the origin toward the positive

axis) of the PDFs illustrate the dominance in entropy production events over innate entropy consumption processes and follow SSFT for a smaller timescale than mean free relaxation time. From the SSFT, the average entropy at shear stress 0.0025 Pa and 0.0020 Pa has been estimated as $(1.7535 \pm 0.096) \text{ s}^{-1}$ and $(1.2517 \pm 0.089) \text{ s}^{-1}$, respectively. This indicates that a large mass of participating constituents exhibits velocity gradient fluctuations as compared to the Brownian system. Again, in terms of energy metric, it has been quantified through the effective temperature, T_{eff} , which increases with global power flux. This predicts the shear-driven athermal nature of the NEQ fluctuation. The validation of thermodynamic uncertainty relation (TUR) for our sheared Hb system reveals the existence of the bounding nature of the NEQ in the aggregate state. This may open up new avenues in the field of the flow behavior of complex bio-molecular systems for molecular fluidic device applications.

Acknowledgements A.K. would like to acknowledge the University Grant Commission, India, for financial support, UGC-Ref. No. 1401/(CSIR-UGC NET JUNE 2017). The CIF, IIT Bhubaneswar, is acknowledged for support during the rheological studies.

Author contributions

AK was involved in conceptualizations, data accusation, methodology, formal analysis, writing, and review and editing. GM was involved in validation and resources. PPD and PK were involved in resources. MKB was involved in review and writing. SR was involved in supervision, conceptualization, formal analysis, validation, writing, and review and editing.

Data availability The data supporting the findings of this study are available within the article and as a supplementary file and any other data can be made available on reasonable request.

Declarations

Conflict of interest The authors have no conflicts of interest to disclose.

References

1. E. Lauga, T.R. Powers, Rep. Prog. Phys. **72**, 096601 (2009)
2. D.L. Koch, G. Subramanian, Annu. Rev. Fluid Mech. **43**, 637 (2011)
3. S. Nambiar, P.R. Nott, G. Subramanian, J. Fluid Mech. **812**, 41 (2017)
4. A.M. Stadler, I. Digel, G.M. Artmann, J.P. Embs, G. Zaccai, G. Büldt, Biophys. J. **95**, 5449 (2008)
5. R. Bhomia, V. Trivedi, N.J. Coleman, J.C. Mitchell, J. Pharm. Anal. **6**, 242 (2016)
6. I.C. Tsimouri, P.S. Stephanou, V.G. Mavrantzas, Phys. Fluids **30**, 030710 (2018)
7. E. Nader, S. Skinner, M. Romana, R. Fort, N. Lemonne, N. Guillot, A. Gauthier, S. Antoine-Jonville, C. Renoux, M.D. Hardy-Dessources, E. Stauffer, P. Joly, Y. Bertrand, P. Connes, Front. Physiol. **10**, 1 (2019)
8. S. Atwell, C. Badens, A. Charrier, E. Helfer, A. Viallat, Front. Physiol. **12**, 1 (2022)
9. J.M. Higgins, D.T. Eddington, S.N. Bhatia, L. Mahadevan, PLoS Comput. Biol. **5**, 1 (2009)
10. K.N. Morshed, D. Bark, M. Forleo, L.P. Dasi, PLoS ONE **9**, 1 (2014)
11. D.J. Evans, D.J. Searles, Phys. Rev. E **50**, 1645 (1994)
12. G. Gallavotti, E.G.D. Cohen, J. Stat. Phys. **80**, 931 (1995)
13. G. Gallavotti, E.G.D. Cohen, Phys. Rev. Lett. **74**, 2694 (1995)
14. R. van Zon, E.G.D. Cohen, Phys. Rev. Lett. **91**, 1 (2003)
15. S. Majumdar, A.K. Sood, Phys. Rev. E **85**, 041404 (2012)
16. N. Kumar, S. Ramaswamy, A.K. Sood, Phys. Rev. Lett. **106**, 18 (2011)
17. D.J. Sivananda, N. Roy, P.C. Mahato, S.S. Banerjee, Phys. Rev. Res. **2**, 1 (2020)
18. C. Jarzynski, Phys. Rev. Lett. **78**, 2690 (1997)
19. S. Majumdar, A.K. Sood, Phys. Rev. Lett. **101**, 078301 (2008)
20. J.M. Horowitz, T.R. Gingrich, Nat. Phys. **16**, 15 (2020)
21. A.M. Timpanaro, G. Guarnieri, J. Goold, G.T. Landi, Phys. Rev. Lett. **123**, 1 (2019)
22. A.C. Barato, U. Seifert, Phys. Rev. Lett. **114**, 1 (2015)
23. Z. Cao, J. Su, H. Jiang, Z. Hou, Phys. Fluids **34**, 053310 (2022)
24. S. Ikeda, K. Nishinari, Food Hydrocoll. **15**, 401 (2001)
25. V. Sharma, A. Jaishankar, Y.C. Wang, G.H. McKinley, Soft Matter **7**, 5150 (2011)
26. R. G. Larson, *The Structure and Rheology of Complex Fluids* (OUP USA, 1999)
27. V. Carrier and G. Petekidis, J. Rheol. (N. Y. N. Y). **53**, 245 (2009)
28. S. M. Fielding, P. Sollich, and M. E. Cates, J. Rheol. (N. Y. N. Y). **44**, 323 (2000)
29. S. Majumdar, A.K. Sood, Soft Matter **7**, 7805 (2011)
30. P.C.F. Møller, A. Fall, D. Bonn, EPL **87**, 38004 (2009)
31. A. Malkin, S. Ilyin, A. Semakov, V. Kulichikhin, Soft Matter **8**, 2607 (2012)
32. P. Coussot, Q. D. Nguyen, H. T. Huynh, and D. Bonn, J. Rheol. (N. Y. N. Y). **46**, 573 (2002)
33. A.N. Alexandrou, N. Constantinou, G. Georgiou, J. Nonnewton, Fluid Mech. **158**, 6 (2009)
34. A. Rafe, R. Seddighi, M. Mousavi, E. Bastan, Legum. Sci. **5**, 1 (2023)
35. J. Shim, S.J. Mulvaney, J. Sci. Food Agric. **81**, 706 (2001)

36. B. Bag, G. Shaw, S.S. Banerjee, S. Majumdar, A.K. Sood, A.K. Grover, *Sci. Rep.* **7**, 1 (2017)
37. H. Li, X. Yang, H. Zhang, H. Zhang, *Chin. Phys. B* **29**, 060502 (2020)
38. P. Dolai, A. Simha, *J. Stat. Mech. Theory Exp.* **2016**, 083203 (2016)
39. J. A. Drocco, C. J. Olson Reichhardt, and C. Reichhardt, *Eur. Phys. J. E* **34**, 117 (2011)
40. K. Feitosa, N. Menon, *Phys. Rev. Lett.* **92**, 1 (2004)

Springer Nature or its licensor (e.g. a society or other partner) holds exclusive rights to this article under a publishing agreement with the author(s) or other rightsholder(s); author self-archiving of the accepted manuscript version of this article is solely governed by the terms of such publishing agreement and applicable law.